

A new design and simulation of an aberration-corrected PEEM/ARPES/nano-ARPES instrument

Yuqin Yang(杨玉琴), Zichun Miao(苗滋春), Shan Qiao(乔山), Wenxin Tang(唐文新), Ning Dai(戴宁), and Weishi Wan(万唯实)

Citatio: Chin. Phys. B, 2025, 34 (**9**): 094101. DOI: 10.1088/1674-1056/adebed
http://cpb.iphy.ac.cn; http://iopscience.iop.org/cpb

What follows is a list of articles you may be interested in

Design of an all-dielectric long-wave infrared wide-angle metalens

Ning Zhang(张宁), Qingzhi Li(李青芝), Jun Chen(陈骏), Feng Tang(唐烽),Jingjun Wu(伍景军), Xin Ye(叶鑫), and Liming Yang(杨李茗)

Chin. Phys. B, 2022, 31 (**7**): 074212. DOI: 10.1088/1674-1056/ac4026

Optical design of common-aperture multispectral and polarization optical imaging system with wide field of view

Xin Liu(刘鑫), Jun Chang(常军), Shuai Feng(冯帅), Yu Mu(穆郁), Xia Wang(王霞), Zhao-Peng Xu(徐兆鹏)

Chin. Phys. B, 2019, 28 (**8**): 084201. DOI: 10.1088/1674-1056/28/8/084201

Aberration correction of conformal dome based on rotated cylindrical lenses for ultra-wide field of regard

Linyao Yu(虞林瑶), Yongfeng Hong(洪永丰), Zhifeng Cheng(程志峰), Bao Zhang(张保)

Chin. Phys. B, 2018, 27 (**1**): 014202. DOI: 10.1088/1674-1056/27/1/014202

Wavefront reconstruction algorithm for wavefront sensing based on binary aberration modes

Boqing Pang(庞博清), Shuai Wang(王帅), Tao Cheng(程涛), Qingfeng Kong(孔庆峰), Lianghua Wen(文良华), Ping Yang(杨平)

Chin. Phys. B, 2017, 26 (**5**): 054204. DOI: 10.1088/1674-1056/26/5/054204

Femtosecond electron pulse compression by using the time focusing technique in ultrafast electron diffraction

Wen Wen-Long(温文龙), Lei Xiao-Hong(雷晓红), Hu Xin(胡昕), Xu Xiang-Yan(徐向晏), Wang Jun-Feng(王俊锋), Cao Xi-Bin(曹希斌), Liu Hu-Lin(刘虎林), Wang Chao(王超), Dang Li-Hong(党利宏), and Tian Jin-Shou(田进寿)

Chin. Phys. B, 2011, 20 (**11**): 114102. DOI: 10.1088/1674-1056/20/11/114102

INSTRUMENTATION AND MEASUREMENT

A new design and simulation of an aberration-corrected PEEM/ARPES/nano-ARPES instrument

Yuqin Yang(杨玉琴)[1], Zichun Miao(苗滋春)[2], Shan Qiao(乔山)[3,1], Wenxin Tang(唐文新)[2], Ning Dai(戴宁)[4,1,†], and Weishi Wan(万唯实)[5,1,‡]

[1] *ShanghaiTech University, Shanghai* 201210, *China*
[2] *Suzhou AISTech Co., Ltd., Suzhou* 215133, *China*
[3] *State Key Laboratory of Functional Materials for Informatics, Shanghai Institute of Microsystem and Information Technology, Chinese Academy of Sciences, Shanghai* 200050, *China*
[4] *Shanghai Institute of Technical Physics of the Chinese Academy of Science, Shanghai* 200083, *China*
[5] *Quantum Science Center of Guangdong–Hong Kong–Macao Greater Bay Area, Shenzhen* 518045, *China*

(Received 11 April 2025; revised manuscript received 24 June 2025; accepted manuscript online 4 July 2025)

Over the past few decades, angle-resolved photoemission spectroscopy (ARPES) has been one of the important tools to study electronic structure of crystals. In recent years, the spatial resolution of around 150 nm has been reached through tight focusing of the light spot (nano-ARPES). At present, the lower limit of the spot size of the light on the sample has been reached. Another way to further improve the spatial resolution is through using apertures to only let electrons from a small area of the sample pass. With both back-focal plane and image apertures, the size of the selected area can be as small as 20 nm. Yet, without aberration correction, the maximum opening angle at the sample for 20 nm spatial resolution is usually smaller than 3°, making this method not suitable for nano-ARPES. As shown in this paper, a conventional aberration corrector, which corrects chromatic and third-order spherical aberrations, is not enough either. Only when the fifth-order spherical aberration is also corrected, the opening angle at the sample is large enough for nano-ARPES. In this paper, the design of a time-of-fight PEEM/ARPES/nano-ARPES instrument, which is currently under development at the Quantum Science Center of Guangdong–Hong Kong–Macao Greater Bay Area, is presented. The main point of innovation is a five-electrode electron mirror corrector, which is used to correct simultaneously chromatic, third-order and fifth-order spherical aberrations, resulting in 1 nm spatial resolution with $\sim$ 230 mrad aperture angle in PEEM mode. This makes feasible the method of using apertures to improve the spatial resolution of the nano-ARPES mode. A new design of the magnetic prism array (MPA) is also presented, which preserves the rotational symmetry better than the existing designs.

Keywords: electrostatic lenses, aberrations, photoemission and photoelectron spectra

PACS: 41.85.Ne, 42.15.Fr, 79.60.–i

DOI: 10.1088/1674-1056/adebed **CSTR:** 32038.14.CPB.adebed

1. Introduction

Photo-in-electron-out process, based on the photoelectric effect and first observed by Hertz in 1887,[1] is an important tool for investigating material properties in real and momentum spaces. The commonly used methodologies based on the photoelectric effect are photoemission electron microscopy (PEEM)[2,3] and angle-resolved photoemission electron spectroscopy (ARPES).[4] The former has been widely used in characterizing micro-nano plasmonic functional devices,[5] high-order plasmonic vortex fields,[6] plasmonic skyrmions[7] and low-dimensional semiconductor materials.[8] The latter is a crucial technique for investigating the electronic states of crystals, including topological materials[9] and low-dimensional systems.[10] These methods enable researchers to gain insight into the fundamental principles of the physical phenomenon of these materials. The significance of photoemission spectroscopy and microscopy is underscored by the establishment of numerous synchrotron-based beamlines around the world,[11–15] which provide the high-intensity light necessary for precise measurements. In addition, a spin filter can be implemented to study the spin-polarized electronic structure of magnetic domains.[16,17] In a nutshell, a PEEM/ARPES instrument can function as an effective tool to investigate local electronic states in energy-, momentum-, spin- and real-spaces.

One of the recent developments of ARPES is combining real- and momentum-space resolutions, which is called nano-ARPES. Specifically, a special lens, such as a zone plate, is used to focus the light further, as a result, the spot size is reduced by roughly two orders of magnitude to around 50–150 nm.[4] Nano-ARPES instruments enable the study of local variations of electronic properties and it is desirable to im-

†Corresponding author. E-mail: ndai@mail.sitp.ac.cn
‡Corresponding author. E-mail: wanweishi@quantumsc.cn

© 2025 Chinese Physical Society and IOP Publishing Ltd. All rights, including for text and data mining, AI training, and similar technologies, are reserved.

prove the spatial resolution further so that smaller areas can be studied. To the best of our knowledge, there is no way of reducing the light spot further. Another way to further improve the spatial resolution is through using apertures to only let electrons from a small area of the sample pass. With both back-focal plane (angle) and image (field) apertures, the size of the selected area can be as small as 20 nm. Yet, without aberration correction, the maximum opening angle at the sample for 20 nm spatial resolution is usually smaller than 3°, making this method not suitable for nano-ARPES. As shown in this paper, a conventional aberration corrector, which corrects chromatic and third-order spherical aberrations, is not enough either. Only when the fifth-order spherical aberration is also corrected, the opening angle at the sample is large enough for nano-ARPES.

Meanwhile, aberrations limit the spatial resolution of PEEM instruments.[18] Various aberration correction methods have been proposed for electron microscopes,[19–27] and the most commonly employed approach for PEEM involves using an electron mirror and a magnetic prism array (MPA).[28–30] In addition, conventional ARPES instruments that utilize hemispherical analyzers often struggle to achieve high throughput, constraining their effectiveness in detailed electronic structure studies. Furthermore, hemispherical analyzers are rather difficult to manufacture, making ARPES instruments less accessible to users.

To address these limitations, a novel time-of-fight PEEM/ARPES/nano-ARPES instrument is under development at the Quantum Science Center of Guangdong–Hong Kong–Macao Greater Bay Area, which uses an electron mirror to correct important aberrations and a time-of-fight analyzer to measure the energy and momentum of the electrons. The key point of innovation is a five-electrode electron mirror corrector, which is used to correct chromatic, third-order and fifth-order spherical aberrations simultaneously, resulting in 1 nm spatial resolution with $\sim$ 230 mrad aperture angle in PEEM mode. This makes feasible the method of using apertures to improve the spatial resolution of the nano-ARPES mode. A new design of the magnetic prism array (MPA) is also presented, which preserves the rotational symmetry better than the existing designs. The electron optics design is presented in Section 2 and simulation results are shown in Section 3. Conclusions and future work are discussed in Section 4.

2. Electron optics design of the instrument

The layout of the time-of-fight PEEM/ARPES/nano-ARPES instrument is shown in Fig. 1. Photoelectrons generated by a pulsed laser are emitted from the sample and accelerated by the objective lens to 5 keV. A five-electrode electron mirror and an MPA are employed to correct the lowest-order chromatic aberration, as well as the third- and fifth-order spherical aberrations, where the electrons are bent 90° after the first pass of the MPA, reflected by the electron mirror and bent 90° again after the second pass of the MPA (see Fig. 2 for more details of the electron optical paths). Unlike most other PEEMs, which usually accelerate electrons to 15 keV or 20 keV, the lower accelerating voltage reduces technical difficulty, but increases the contribution of aberrations from the MPA, making its design more challenging. Furthermore, the sample is grounded while the column is floated on high voltage, making it easier to cool the sample to liquid helium temperature. After the second pass of the MPA, the electrons are focused by a transfer lens with relatively long focal length ($\sim$ 10 cm), forming an intermediate image with magnification of roughly 55, where a field aperture is placed for area selection of the nano-ARPES mode. Meanwhile, an angle aperture is placed at the diffraction plane of the transfer lens to limit the maximum initial angle of the electrons reaching the detector (see Fig. 1 for details). The nano-ARPES mode is realized through the combination of the angle and the field apertures, where only electrons emitted from a small area on the sample are transmitted. After going through another transfer lens, the electrons are decelerated to $\sim$ 1.5 eV and travel $\sim$ 1 m to the delay line detector with $\sim$ 150 ps time resolution, where both time-of-flight and transverse position of an electron can be measured.

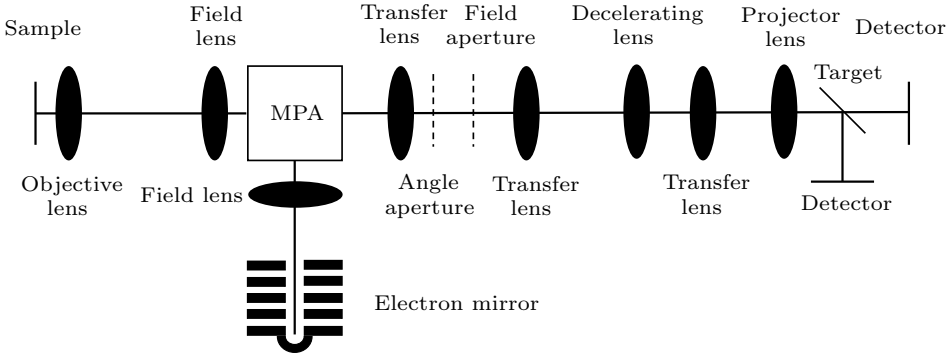


Fig. 1. The schematic diagram of the PEEM/ARPES/nano-ARPES instrument.

The principal rays of imaging (PEEM) and diffraction (ARPES) modes are presented in Fig. 2, where the image plane and the diffraction planes are placed at the detector, respectively. Specifically, for the imaging mode, the objective lens forms an image at the entrance of the MPA and the field lens places the diffraction plane at the center of the MPA. Note that the diffraction plane shown in Fig. 2 at the geometric center of the MPA is the virtual image of the real diffraction plane, which is at the midpoint of the curved optical axis and not shown. As a result, the axial ray is symmetric about the center of the MPA and the field ray is antisymmetric, which maximizes the number of aberrations cancelled by symmetry. The field lens between the MPA and the electron mirror places the diffraction plane at the turning point of the electron mirror so that the field ray is not significantly affected by the electron mirror. This arrangement allows for correcting aberrations without significantly reducing the field of view. Apart from correcting the 3 aberrations, the electron mirror also places the image plane at the exit of the MPA (the image plane before the electron mirror). Altogether, as in the MPA, the axial and field rays in the electron mirror are symmetric and antisymmetric, respectively. As stated above, the first transfer lens downstream of the MPA (after the second pass) forms an intermediate image where the field aperture can be placed and a diffraction plane where the angle aperture can be placed. The transfer lens downstream of the field aperture magnifies the image by a factor of around 5 and places it in front of the decelerating lens. Finally, the last two lenses (transfer lens and projector lens) magnify the image further and place it at the detector. For the diffraction mode, most of the optics is the same, except for the last two lenses, where the diffraction plane is placed at the detector.

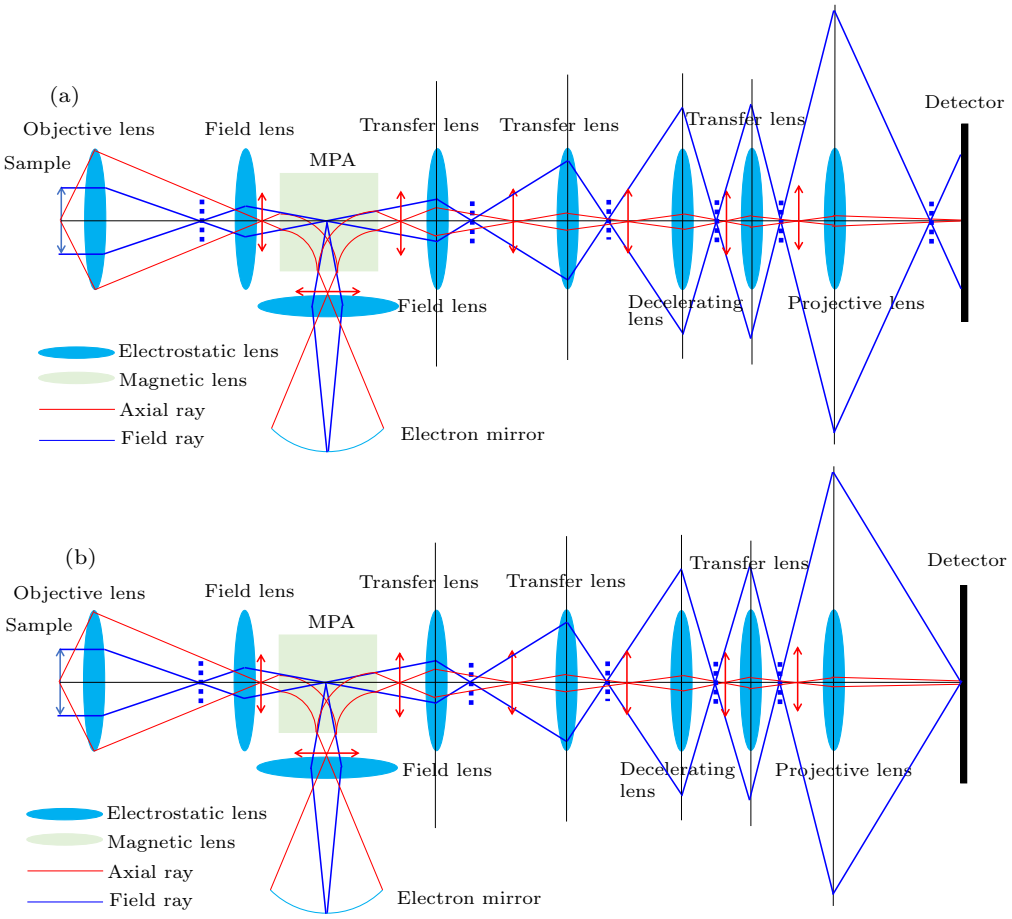


Fig. 2. The principal rays of the time-of-flight PEEM/ARPES/nano-ARPES instrument, (a) the imaging (PEEM) mode; (b) the diffraction (ARPES) mode. The blue lines indicate the trajectories of the field rays; the red lines indicate the trajectories of the axial rays. The red double arrows indicate the locations of the image planes and the dotted blue line segments indicate those of the diffraction planes.

Except for the MPA, all the lenses in this instrument are electrostatic round lenses (see Fig. 3). Since all round lenses apart from the objective lens and the electron mirror are similar in layout, only one type of them is shown in Fig. 3.

As mentioned above, lower accelerating voltage increases the challenge of designing the MPA. The main challenge is to come up with a design that retains as much as possible the rotational symmetry, which will reduce the magnitude of the remaining chromatic and spherical aberrations after correction. Our new design shown in Fig. 4 advances significantly in that direction. The main feature of this design is that most of the focusing is produced by the electrostatic round lenses. The

focusing powers of both the bending magnets and the electrostatic quadrupoles are weak in comparison. Like all the other designs of MPA, the field and axial rays are symmetric and anti-symmetric about the midpoint of the MPA, respectively, or vice versa. In other words, the image planes are placed at the entrance and exit, and the diffraction plane is placed at the center of each pass of the MPA as shown in Fig. 2, or the other way around. As a result, both the number and amplitude of the aberrations of the MPA are kept at the minimum.

Due to the presence of nonlinearity in the equations of motion, mainly from the distribution of the electrostatic and magnetic fields, the final position of an electron is inevitably a nonlinear function of its initial position, angle and energy deviation. In other words, aberrations are always present in electron optical systems.[32] Among the numerous aberrations, the lowest-order chromatic and the third-order spherical aberrations are most important, since they are most responsible for limiting the spatial resolution of an imaging system (see Ref. [33] for illustrations of the effect of these two aberrations in a round lens). Furthermore, Scherzer's theorem states that, for round lenses, these two aberrations are of definite signs, i.e., more energetic electrons are always focused less and electrons with larger initial angles are always focused more.[34] As a result, these aberrations can be corrected by introducing one of the following: electrostatic or magnetic multipole fields, reflection, space charges or time-varying fields.[20,35] In practice, only multipole and mirror correctors have been successfully demonstrated and widely employed in electron microscopes.[19–31] For a low-voltage electron microscope, such as a PEEM or a low-energy electron microscope (LEEM), a mirror corrector is the choice for aberration correction, due to its simplicity.[28–31] Up to now, four-electrode mirror correctors are used to correct lowest-order chromatic aberration and third-order spherical aberration. In this paper, we propose a five-electrode mirror corrector that corrects lowest-order chromatic aberration, third- and fifth-order spherical aberrations.

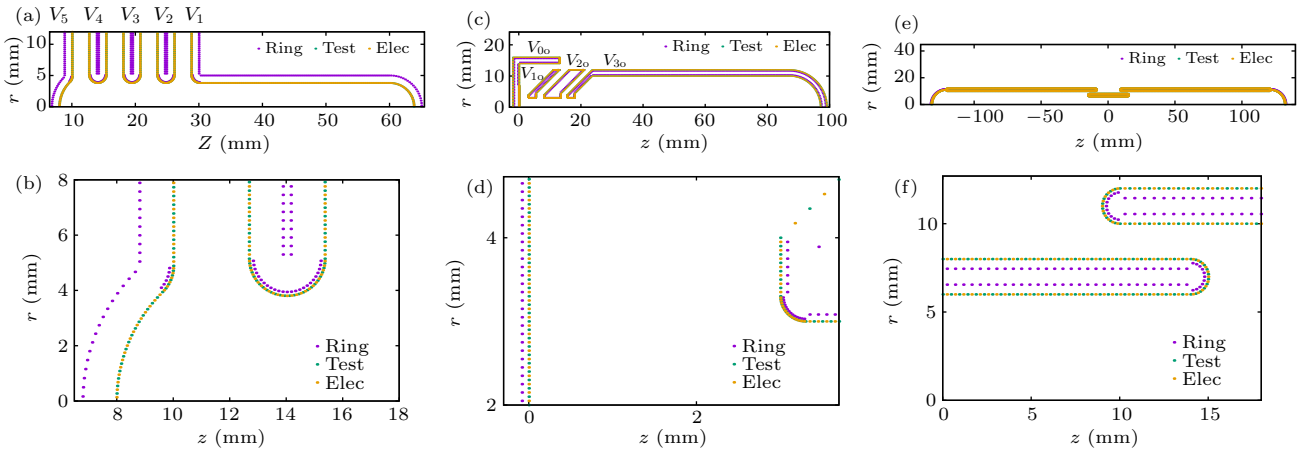


Fig. 3. The charged ring model of round lenses, (a) the electron mirror; (b) the zoomed-in view of one part of the electron mirror; (c) the objective lens; (d) the zoomed-in view of one part of the objective lens; (e) the field lens; (f) the zoomed-in view of one part of the field lens. The labels "ring", "test" and "elec" stand for charged ring, test point and electrode, respectively. For details, see Ref. [31].

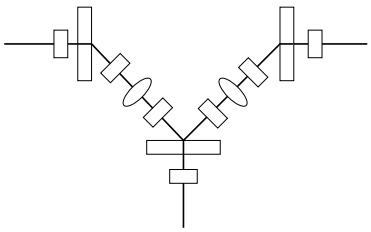


Fig. 4. The layout of the MPA, where long rectangles (two vertical and one horizontal) represent the 45° bending magnets; short rectangles represent the electrostatic quadrupoles and the ovals represent the electrostatic round lenses.

The function of the electron mirror is to correct chromatic and spherical aberrations with as little effect on the field of view as possible. As stated above, the diffraction plane is placed at the turning point where the electrons are reflected. Hence the field ray is anti-symmetric about the turning point and stays close to the optical axis inside the mirror, minimizing the effect of the mirror on the field ray. Meanwhile, the axial ray is symmetric about the turning point and stays far away from the optical axis, reaching maximum radial displacement at the turning point and maximizing the effectiveness of aberration correction.

3. Simulation results

The numerical models of the lenses are implemented in the code COSY INFINITY,[36] which is the first charged particle optics code that employs the differential algebra (DA) technique.[37] Numerically integrating the reference particle through a lens of a charged particle optical system once, all aberrations up to any given order can be obtained, provided that the model of the electromagnetic field is differentiable to the same order or higher. Compared to the traditional ray tracing method, the speed of obtaining aberrations is orders of magnitude higher. Furthermore, COSY INFINITY has an

extremely flexible fitting environment. These factors make COSY INFINITY almost ideal for finding solutions to aberration correction using electron mirror, which happens to be a highly nonlinear and time-consuming process.

All rotationally symmetric (round) lenses are modelled using the charged ring method.[31] The electrostatic quadrupoles are modelled using the hyper-tangent model.[29] The bending magnets are modelled using the Enge model.[38] All of the above models of the electrostatic or magnetic fields are functions that are differentiable to all orders.

Of all the lenses, excluding the mirror, the objective lens contributes the largest amount of the aberrations that limit the instruments' spatial resolution. The fact that the roughness of the sample requires a lower electric field on it further increases the aberrations of the objective lens. As a result, the voltage of V_{1o} (see Fig. 3(c)) is set at ~ 1.5 kV, as opposed to the column voltage of ~ 5 kV, which is commonly done in PEEM. To minimize its aberrations, the high-voltage solution of the objective lens is chosen to form an image at the entrance of the MPA, with the voltage of V_{2o} set at ~ 15 kV. Furthermore, we found that the transfer lens and the projector lens after deceleration also contribute significantly to the aberrations of the whole instrument. Again, high-voltage solutions are adopted for those lenses, which will adversely affect the energy resolution of the instrument.

The electron mirror consists of five electrodes as shown in Fig. 3(a). Let us denote the voltages of the electrodes from right to left as V_1, V_2, V_3, V_4 and V_5, respectively. The fact that the right most electrode is part of the column entails that it is fixed at ~ 5 kV. Since we set the kinetic energy of the reference electron at the sample to be 16 eV, the exact voltage of the column is 4.984 kV. As a result, there are 4 adjustable voltages V_2, V_3, V_4 and V_5 of the mirror. Together with the voltage of the middle electrode of the field lens (V_{2f}) between the MPA and the mirror, there are 5 knobs which are responsible for placing the image plane after the mirror at the location of that before the mirror and the diffraction plane at the turning point of the mirror, as well as correcting the lowest-order chromatic aberration (C_C), the third- and fifth-order spherical aberrations (C_3 and C_5). In addition, the distance between the mirror and the MPA plays an important role in defining the range of the aberrations, since it controls the radial position of the axial ray in the mirror. As a result, it is often included as one of the variables in the fitting process. Obviously, these knobs are not orthogonal to each other and the relations between the variables and the objectives are nonlinear. As a result, the fitting process is largely based on trial and error. After countless setbacks, a family of solutions was found and one of them is listed in Table 1. The stability requirement is obtained assuming the defocus caused by voltage deviation of an electrode is 1 nm on the sample.

Table 1. One of the solutions that correct C_C, C_3 and C_5 simultaneously. $V_{2f} = 2.59768$ kV. The distance between the exit of the MPA and the bottom of the mirror (the point of $z = 0$ in Fig. 3 (middle)) is 533 mm.

	V_2	V_3	V_4	V_5
Voltage (kV)	5.90865	14.04507	16.8303	3.680149
Stability	1.7×10^{-6}	5.7×10^{-7}	4.8×10^{-7}	4.1×10^{-7}

To quantify the robustness of the solution, a parameter scan is performed. On a 3D grid, the values of V_3, V_4 and V_5 are set to change between 10 kV and 18 kV (step size 1 kV), 12 kV and 20 kV (step size 1 kV), as well as -4.0 kV and -3.0 kV (step size 0.1 kV), respectively. At each grid point, the values of V_2 and V_{2f} are varied to find solutions that keep the positions of the image and diffraction planes unchanged. The results are shown in Fig. 5. Figures 5(a)–5(c) show that the range of the aberrations, especially C_5, is rather limited, which becomes more evident when compared with Fig. 4 in Ref. [31]. This implies that the present family of solutions may not be optimal. In other words, C_5 is largely determined by the distance between the mirror and the MPA. It would be ideal if a new family of solutions with larger range of the aberrations can be found. With the present family of solutions, adding one additional lens between the MPA and the mirror can, in principle, remove the dependence of the aberrations (especially C_5) on the distance between the mirror and the MPA.

The spatial resolution of the instrument is estimated using the formula

$$r = \left[\left(\frac{0.61\lambda}{\alpha}\right)^2 + \left(\frac{1}{4}C_3\alpha^3\right)^2 + \left(C_5\alpha^5\right)^2 + \left(C_7\alpha^7\right)^2 + (C_C\alpha\delta)^2 + \left(C_{CC}\alpha\delta^2\right)^2 + \left(C_{3C}\alpha^3\delta\right)^2\right]^{1/2}, \quad (1)$$

where λ is the wavelength of the electron at the sample, α is the angle acceptance at the sample (aperture angle), C_7 is the seventh-order spherical aberration and $\delta = \Delta E/E_k$ is the relative energy spread. C_{CC} and C_{3C} are two aberrations that contribute significantly to the resolution. The results are shown in Fig. 6. The left plot is the resolution of the imaging (PEEM) mode, since the time-of-flight analyzer can distinguish electrons with more than 5 meV energy deviation. The right plot is the resolution of the nano-ARPES mode, since there is no energy selection at the field aperture. It is worth noting that, although correcting C_5 in addition to C_C and C_3 does improve resolution in the PEEM mode, the main benefit for correcting C_5 is that it significantly improves resolution at the aperture angle ~ 270 mrad, from 285 nm of the uncorrected case to 3.3 nm of the case where C_C, C_3 and C_5 are corrected. This makes feasible the scheme of using angle and field apertures to achieve high spatial resolution in the nano-ARPES mode.

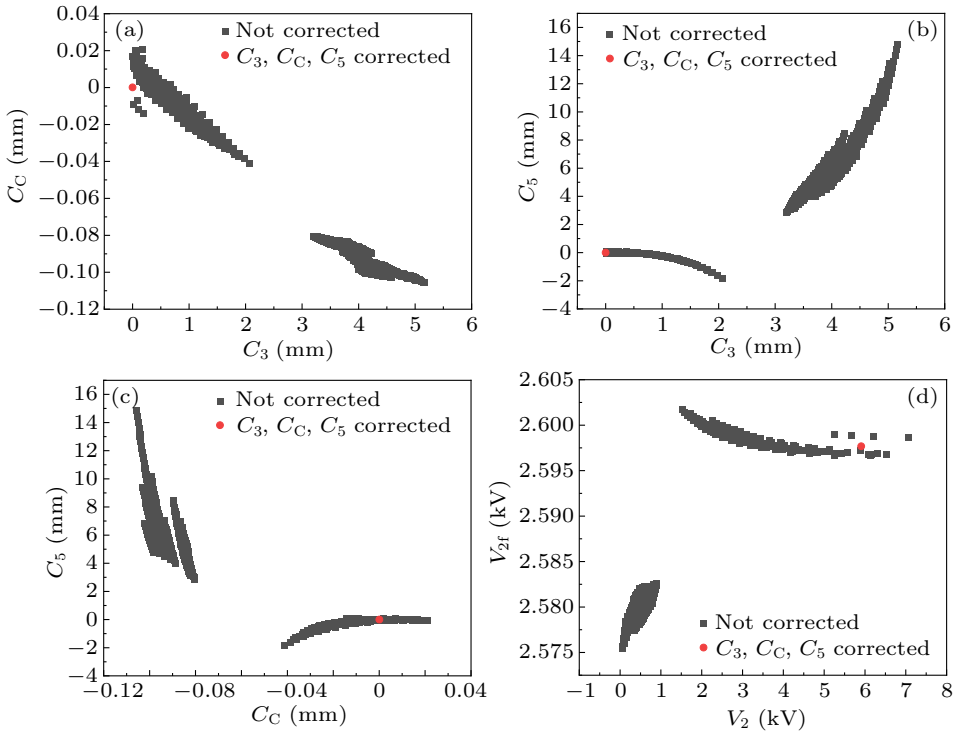


Fig. 5. The values of the aberrations C_C, C_3 and C_5, as well as that of V_{2f}, on the grid of V_3, V_4, and V_5, shown on various projection planes. (a) C_C versus C_3; (b) C_5 versus C_3; (c) C_5 versus C_C; (d) V_{2f} versus V_2.

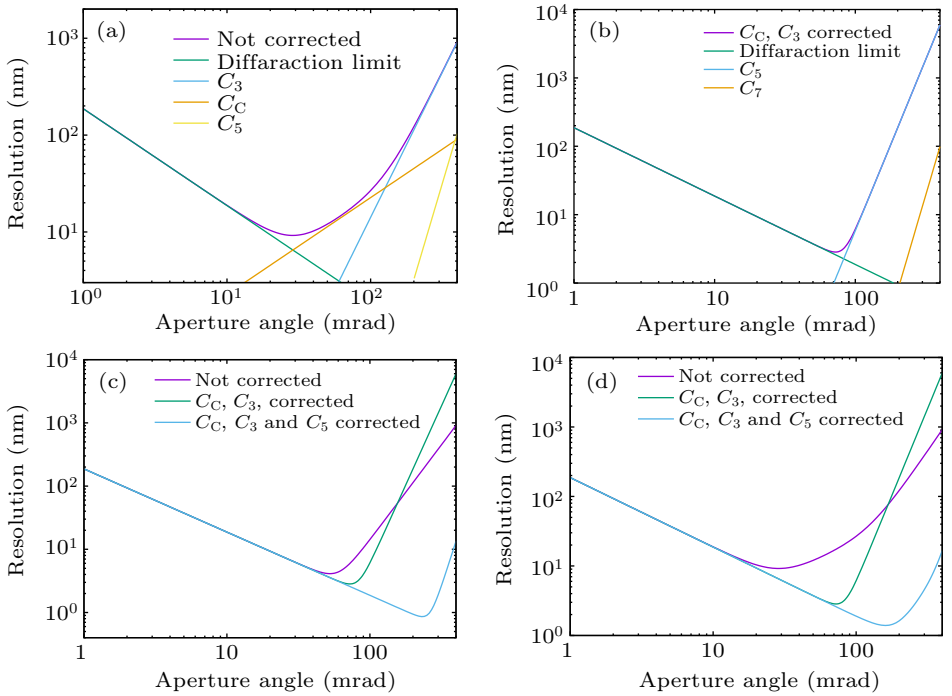


Fig. 6. The resolution as a function of the aperture angle. (a) Aberration not corrected (straight), $\delta = 200$ meV, showing the effects of important aberrations; (b) C_C and C_3 corrected, $\delta = 200$ meV, showing the effects of important aberrations; (c) aberration not corrected, C_C and C_3 corrected, as well as C_C, C_3 and C_5 corrected, $\delta = 5$ meV; (d) aberration not corrected, C_C and C_3 corrected, as well as C_C, C_3 and C_5 corrected, $\delta = 200$ meV.

To further understand the performance of this instrument, a start-to-end tracking study is done. For a single-pass system, tracking can be done using the high-order transfer map.[39] Specifically, the 7th order transfer map from the sample to the detector is generated by concatenating the transfer maps of the lenses and an ensemble of electrons is tracked through it. The positions of the electrons on the detector are recorded and plotted. The electrons are emitted on the optical axis with different slopes and energy. The average kinetic energy is 16 eV and the distribution of energy deviation is Gaussian with $\sigma_E = 2.5$ meV and a cutoff at 2.5 sigma. The maximum angles of the electrons at the sample are 3.0°, 4.1° and 13.2° for

the cases of aberration not corrected, C_C and C_3 corrected and C_C, C_3 and C_5 corrected, respectively. The distribution of the angles is a square grid limited by a circle whose radius is the maximum angle. The grid lengths are 0.1°, 0.1° and 0.5° for the above three cases, respectively. The results are displayed in Fig. 7, where the effect of aberration correction is clearly shown by the reduction of the size of the beam spot. The apparent star shape of the beam spot in the right picture indicates that the MPA contributes most of the remaining aberrations. Upon closer inspection, the most prominent remaining aberrations are 6th- and 7th-order spherical aberrations. Note that the 6th-order spherical aberrations can only be produced by the MPA.

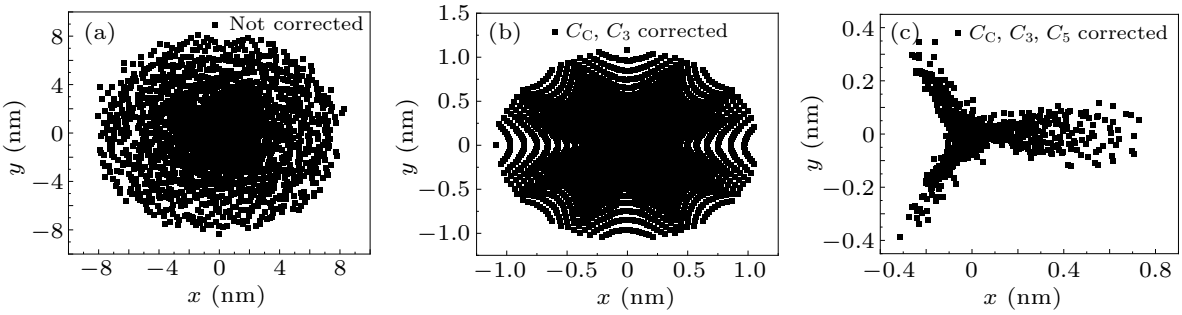


Fig. 7. Start-to-end tracking results of the imaging (PEEM) mode. (a) Aberration not corrected, (b) C_C and C_3 corrected, (c) C_C, C_3 and C_5 corrected.

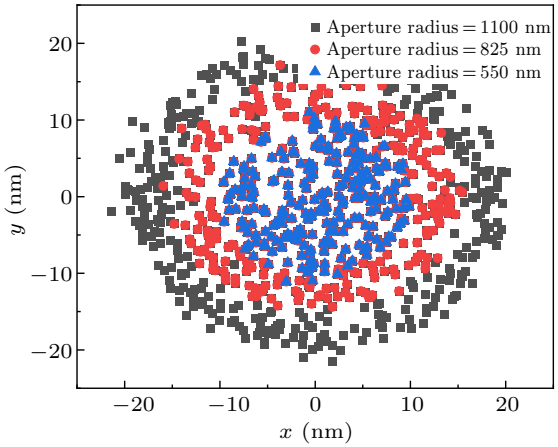


Fig. 8. Distribution of transmitted electrons on the sample at different radii of the field aperture. The initial position distribution is Gaussian with $\sigma_r = 150$ nm and a cutoff at 2.5 sigma. The energy distribution is Gaussian with $\sigma_E = 100$ meV and a cutoff at 2.5 sigma. The initial angle distribution is Gaussian with $\sigma_\alpha = 15°$ and a cutoff at 1 sigma.

Conventional nano-ARPES technique relies on focusing the light beam more strongly to achieve smaller spot size on the sample, so that better resolution can be obtained. At present, the smallest laser spot size on the sample is around 150 nm. Here we propose a scheme, which can potentially improve spatial resolution by an order of magnitude, through the combination of a field aperture and an angle aperture (see Fig. 1). As shown in the right picture of Fig. 6, when the aberrations of C_C, C_3 and C_5 are corrected, the spatial resolution at the aperture angle of 270 mrad is about 3.3 nm. The combination of large aperture angle and high spatial resolution makes it possible to operate the instrument in nano-ARPES mode with spatial resolution below 10 nm. The effectiveness of selecting the area of observation by the field aperture is shown in Fig. 8. Since the magnification at the field aperture is 55, a 550 nm radius aperture can limit the area where the transmitted electrons emit to a disk with 10 nm radius (see Fig. 8).

To demonstrate the angle resolution of the nano-ARPES mode, a start-to-end tracking study is performed with the 550 nm radius field aperture in place. The results are shown in Fig. 9. In each case, two bunches of electrons with two slightly different initial angles are tracked from the sample to the detector. The initial position distribution is Gaussian with $\sigma_r = 150$ nm and a cutoff at 2.5 sigma. The energy distribution is Gaussian with $\sigma_E = 2.5$ meV and a cutoff at 2.5 sigma. Figure 9 demonstrates that, for electrons emitting from a 10 nm radius area, the angle resolution can reach 0.1°. Obviously, angle resolution gets better with a smaller area of emitted electrons (higher spatial resolution). Yet the drawback is fewer electrons emitted, which leads to longer data acquisition time and degradation of both angle and spatial resolution due to time dependent fluctuations and drifts of the instrument, such as voltage stability and mechanical vibrations.

The angle resolution of the diffraction (ARPES) mode is worse than that of the nano-ARPES mode due to the larger area where the photoelectrons are emitted. The simulation results are presented in Fig. 10. The initial position distribution is Gaussian with $\sigma_r = 150$ nm and a cutoff at 2.5 sigma. The energy distribution is Gaussian with $\sigma_E = 1.5$ meV and a cutoff at 2.5 sigma. The field aperture is not present. Figure 10 shows that the angle resolution is roughly 0.5°, which is much worse than that of a commercial ARPES instrument since the laser spot size is on the order of 10 μm. One promising path forward is to correct the main aberrations using the mirror corrector by placing the diffraction plane at the entrances and exits of the MPA and the image plane at the turning point of the mirror.

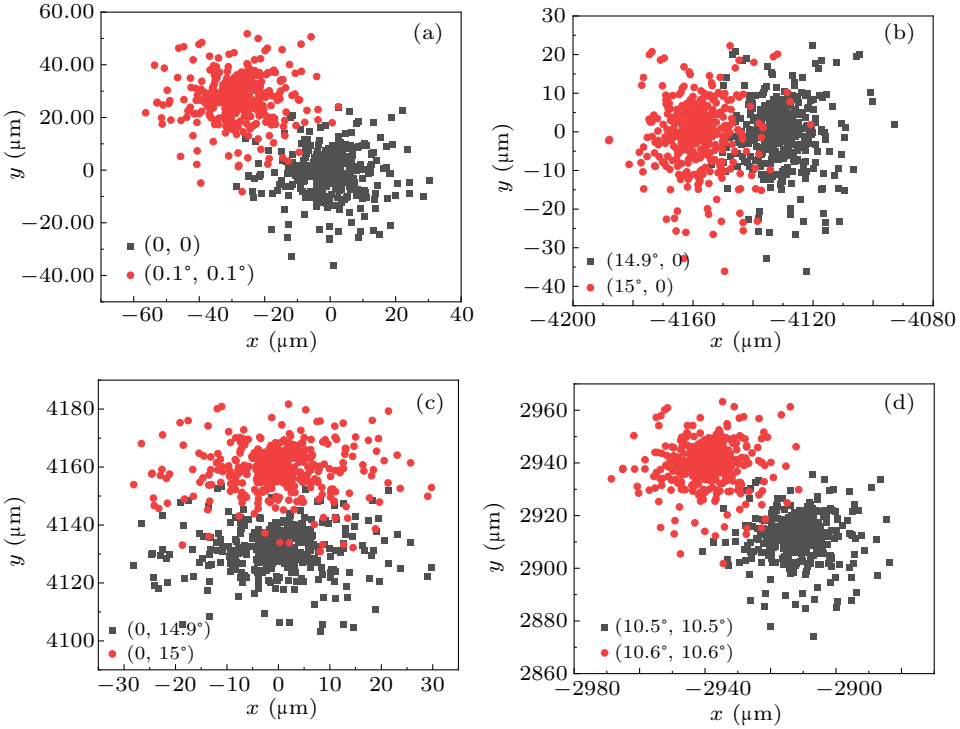


Fig. 9. The start-to-end tracking results of the nano-ARPES mode. The initial position distribution is Gaussian with $\sigma_r = 150$ nm and a cutoff at 2.5 sigma. The energy distribution is Gaussian with $\sigma_E = 2.5$ meV and a cutoff at 2.5 sigma. (a) $\alpha_{x1} = \alpha_{y1} = 0$, $\alpha_{x2} = \alpha_{y2} = 0.1°$; (b) $\alpha_{x1} = 14.9°$, $\alpha_{y1} = 0°$, $\alpha_{x2} = 15°$, $\alpha_{y2} = 0°$; (c) $\alpha_{x1} = 0°$, $\alpha_{y1} = 14.9°$, $\alpha_{x2} = 0°$, $\alpha_{y2} = 15°$; (d) $\alpha_{x1} = \alpha_{y1} = 10.5°$, $\alpha_{x2} = \alpha_{y2} = 10.6°$.

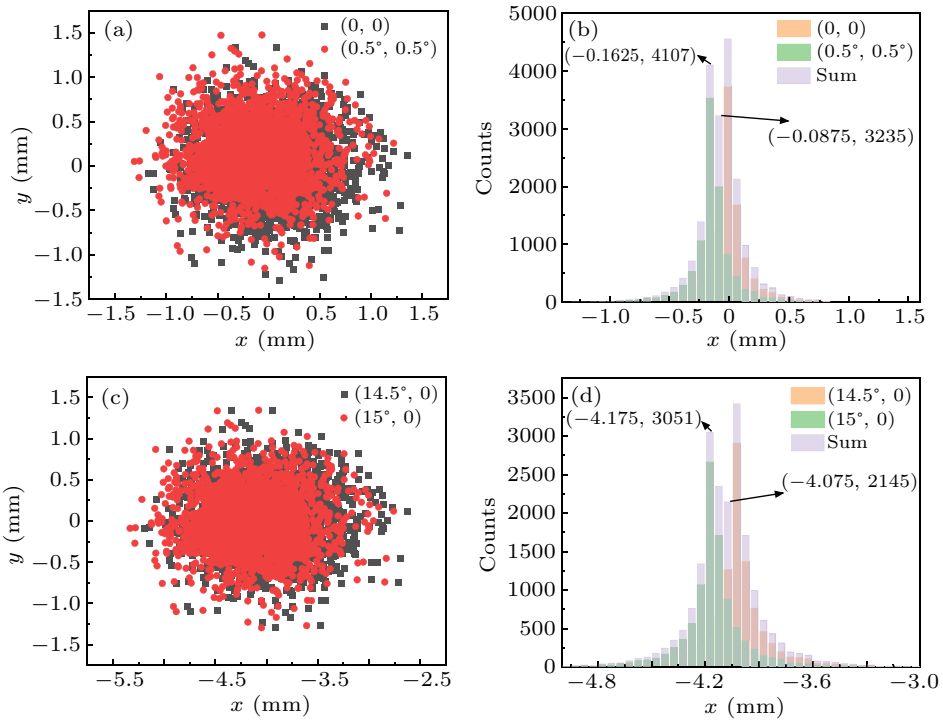


Fig. 10. The resolution of the ARPES mode. The left column is scatter charts of different angles. The right column is histograms along the x-axis. The initial position distribution is Gaussian with $\sigma_r = 150$ nm and a cutoff at 2.5 sigma. The energy distribution is Gaussian with $\sigma_E = 1.5$ meV and a cutoff at 2.5 sigma. (a) and (b) $\alpha_{x1} = \alpha_{y1} = 0°$, $\alpha_{x2} = \alpha_{y2} = 0.5°$; (c) and (d) $\alpha_{x1} = 14.5°$, $\alpha_{y1} = 0°$, $\alpha_{x2} = 15°$, $\alpha_{y2} = 0°$.

4. Conclusions

The design of a novel aberration-corrected PEEM/ARPES/nano-ARPES instrument is presented. A five-electrode electron mirror corrector is used to correct the chromatic, third-order and fifth-order spherical aberrations simultaneously, which results in 1 nm spatial resolution with ~ 230 mrad aperture angle in the PEEM mode. A new design of the MPA is also presented, which preserves the rotational symmetry better than the existing designs. These innovations make it possible to push the spatial resolution of the nano-ARPES mode to below 10 nm together with angle and field apertures. In the next step, attempts will be made to correct

the aberrations limiting the angle resolution of the ARPES mode using the electron mirror. In the long run, a new family of more robust solutions for correcting C_C, C_3 and C_5 is highly desirable.

Acknowledgements

The authors would like to acknowledge thought provoking discussions with Dr. Tony Yu and Dr. Fayuan Zhang. This work is supported by ShanghaiTech University and Quantum Science Center of Guangdong–Hong Kong–Macao Greater Bay Area, China (Grant No. SZZX2301006).

References

[1] Dai Y 2024 *Chin. Phys. B* **33** 038703
[2] Feng J and Scholl A 2007 *Science of Microscopy* (Hawkes P W and Spence J C H, Ed.) (New York: Springer) pp. 657–695
[3] Sala A 2020 *Springer Handbook of Surface Science* (Rocca M, Rahman T H and Vattuone L, Ed.) (Cham: Springer) pp. 387–425
[4] Zhang H, Pincelli T, Jozwiak C, Kondo T, Ernstorfer R, Sato T and Zhou S 2022 *Nat. Rev. Methods Primers* **2** 54
[5] Douillard L, Charra F, Korczak Z, Bachelot R, Kostcheev S, Lerondel G, Adam P M and Royer P 2008 *Nano Lett.* **8** 935
[6] Spektor G, Prinz E, Hartelt M, Mahro A K, Aeschlimann M and Orenstein M 2021 *Sci. Adv.* **7** eabg5571
[7] Davis T J, Janoschka D, Dreher P, Frank B, Meyer zu Heringdorf F J and Giessen H 2020 *Science* **368** eaba6415
[8] Man M K L, Margiolakis A, Deckoff-Jones S, Harada T, Wong E L, Krishna M B M, Madéo J, Winchester A, Lei S, Vajtai R, Ajayan P M and Dani K M 2017 *Nat. Nanotechnol.* **12** 36
[9] Lv B, Qian T and Ding H 2019 *Nat. Rev. Phys.* **1** 609
[10] Lu Q, Reddy P V S, Jeon H, Mazza A R, Brahlek M, Wu W, Yang S A, Cook J, Conner C, Zhang X, Chakraborty A, Yao Y T, Tien H J, Tseng C H, Yang P Y, Lien S W, Lin H, Chiang T C, Vignale G, Li A P, Chang T R, Moore R G and Bian G 2024 *Nat. Commun.* **15** 6001
[11] Kang T H, Kim K J, Hwang C C, Rah S, Park C Y and Kim B 2001 *Nucl. Instrum. Meth. Phys. Res. Sect. A* **467–468** 581
[12] Reininger R, Hulbert S L, Johnson P D, Sadowski J T, Starr D E, Chubar O, Valla T and Vescovo E 2012 *Rev. Sci. Instrum.* **83** 023102
[13] Grass M E, Karlsson P G, Aksoy F, Lundqvist M, Wannberg B, Mun B S, Hussain Z and Liu Z 2010 *Rev. Sci. Instrum.* **81** 053106
[14] Avila J, Razado-Colambo I, Lorcy S, Lagarde B, Giorgetta J L, Polack F and Asensio M C 2013 *J. Phys.: Conf. Ser.* **425** 192023
[15] Dudin P, Lacovig P, Fava C, Nicolini E, Bianco A, Cautero G and Barinov A 2010 *J. Synchrotron Radiat.* **17** 445
[16] Tusche C, Krasyuk A and Kirschner J 2015 *Ultramicroscopy* **159** 520
[17] Ji F, Shi T, Ye M, Wan W, Liu Z, Wang J, Xu T and Qiao S 2016 *Phys. Rev. Lett.* **116** 177601
[18] Irène C, Simone L, Florian M, Hugo H, Anna T and Felix B 2021 *Comptes Rendus. Physique, Recent advances in 2D material physics* **22** 107
[19] Orlof J 2009 *Handbook of charged particle optics* (London: CRC press) pp. 209–340
[20] Scherzer O 1947 *Optik* **2** 114
[21] Rempfer G F, Desloge D M, Skoczylas W P and Griffith O H 1997 *Microsc. Microanal.* **3** 14
[22] Henkelman R M and Ottensmeyer F P 1974 *J. Phys. E: Sci. Instrum.* **7** 176
[23] Koshikawa T, Shimizu H, Amakawa R, Ikuta T, Yasue T and Bauer E 2005 *J. Phys.: Condens. Matter* **17** S1371
[24] Neßlinger A 1939 *Jahrb. AEG-Forschung* **6** 83
[25] Hawkes P W and Kasper E 1996 *Principles of Electron Optics* (London: Academic Press) pp. 857–878
[26] Hibino M and Maruse S 1976 *J. Electron Microsc.* **25** 229
[27] Hawkes P W Phil 2009 *Trans. Roy. Soc. A* **367** 3637
[28] Preikszas D and Rose H 1997 *J. Electron Microsc.* **46** 1
[29] Wan W, Feng F and Padmore H A 2006 *Nucl. Instrum. Meth. Phys. Res. A* **564** 537
[30] Tromp R M, Hannon J B, Ellis A W, Wan W, Berghaus A and Schaff O 2010 *Ultramicroscopy* **110** 852
[31] Wan W, Feng J, Padmore H A and Robin D S 2004 *Nucl. Instrum. Meth. Phys. Res. A* **519** 222
[32] Rose H 2012 *Geometrical Charged-Particle Optics* 2nd Ed. (Berlin: Springer-Verlag) Chap. 2, 3, and 5
[33] Wan W 2009 *Proceedings of PAC09* (Vancouver, BC, Canada) pp. 778–782
[34] Scherzer O 1936 *Z. Physik.* **101** 593
[35] Scherzer O 1949 *J. Appl. Phys.* **20** 20
[36] Makino K and Berz M 2006 *Nucl. Instrum. Meth. Phys. Res. A* **558** 346
[37] Berz M 1989 *Part. Accel.* **24** 109
[38] Enge H A 1964 *Rev. Sci. Instrum.* **35** 278
[39] Wan W, Brouwer L, Caspi S, Prestemon S, Gerbershagen A, Schippers J M and Robin D 2015 *Phys. Rev. ST Accel. Beams* **18** 103501